Lawrence Berkeley Laboratory
UNIVERSITY OF CALIFORNIA

Engineering Division

Presented at the 6th FTS Conference 1987,
Vienna, Austria, August 24–28, 1987

Far Infrared Fourier Transform Spectroscopy of Semiconductors

E.E. Haller

July 1987

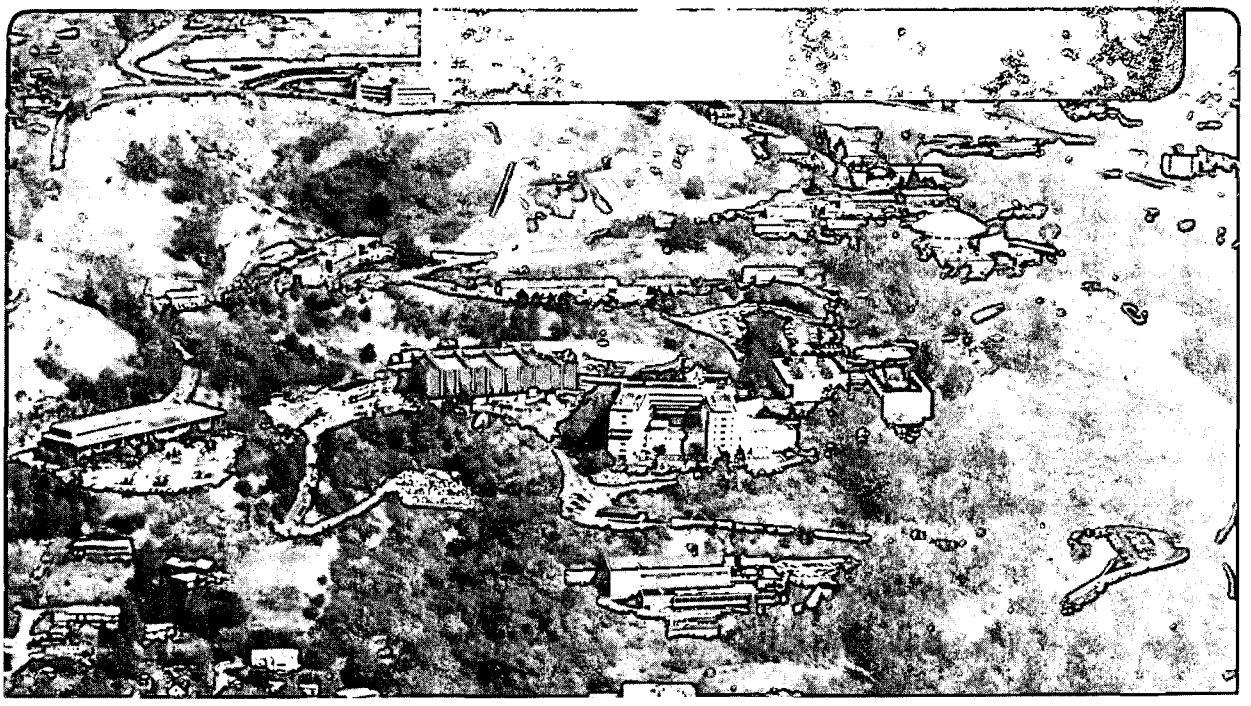

Prepared for the U.S. Department of Energy under Contract DE-AC03-76SF00098

DISCLAIMER

FAR INFRARED FOURIER TRANSFORM SPECTROSCOPY OF SEMICONDUCTORS

Eugene E. Haller

Department of Materials Science and Mineral Engineering and
Lawrence Berkeley Laboratory, University of California
Berkeley, CA 94720 U.S.A.

Abstract

Fourier transform spectrosocpy (FTS) is one of the most important tools in the study of shallow level donors and acceptors in semiconductors. When combined with a two-step photothermal ionization process detected photoconductively, FTS allows measurement of optical transitions of donor-bound electrons (and acceptor-bound holes) in ultra-pure germanium samples with impurity concentrations $< 10^{9}$ cm^{-3} (i.e., one electrically active impurity in 4×10^{13} host atoms). The experimental high resolution study of the hydrogen-like excited state series of shallow levels has yielded as many as 19 lines of width as small as 10 μeV for some centers. These results have stimulated theoretical work which has led to the unambiguous assignment of quantum states to many bound excited states. Extensive studies of ultra-pure Ge crystals grown under different well-controlled conditions have led to the discovery of a large number of novel shallow impurity complexes. Study of the multiplicities and symmetries of the associated electronic states has led to a detailed understanding of the unusual static and dynamic structures of these novel centers. The chemical composition has been deduced from correlations between the concentration of a particular center and the materials involved in crystal growth. Isotopic substitution of hydrogen with deuterium has led to the unambiguous proof of the presence of hydrogen in several of the novel centers. In addition to the high resolution spectra of shallow electronic levels, vibrational spectra of bond-centered interstitial oxygen in ultra-pure Ge are noteworthy for their extraordinarily sharp lines.

1. Introduction

Semiconductors belong to the class of the best understood solids. They can be produced in the form of large single crystals of up to 100 kg in weight with unrivaled perfection and purity. In the most extreme case of ultra-pure germanium, one finds one electrically active impurity in 10^{13} host atoms! Is there then still anything one can learn from such perfect solids or are they simply boring? Indeed, a wealth of most interesting science, both theoretical and experimental, has flowed from the study of semiconductors in the past fifty or so years. This stream of new and exciting results and accompanying discoveries is still growing and there seems to be no downturn in sight. One of the most exciting discoveries obtained with two-dimensional semiconductors in recent years has been the quantized Hall effect for which K. von Klitzing received the 1985 Nobel Prize.

The applications of semiconductor devices in science, medicine, and technology have been so pervasive and are so widely known that I do not attempt to list them here, with one exception, the computer. What would we do with Michelson's interferometer without computers and algorithms which can transform information from one space into another? The answer to this question is as obvious as the one to the inverse question: What would semiconductor physics be without the interferometer? Infrared Fourier Transform Spectroscopy (FTS) and semiconductor physics have benefitted from each other in an unusually productive fashion.

In this paper I will review some of the exciting science which has been performed with semiconductors using FTS. Though a certain personal bias is inescapable, I will try to emphasize unique, spectacular or otherwise important research results.

The variety of photon/semiconductor interactions is very large indeed, and I will group the photon-related excitations into two categories: electronic and vibronic excitations. The former encompasses a broad range of effects including intrinsic ionization and exciton formation, donor and acceptor ionization, and scattering processes, while the latter covers lattice and impurity-related vibrational modes. The development of superb FTS instruments

which cover the electromagnetic spectrum from visible light to mm waves has led to the application of this technique to numerous optical studies. I will emphasize photon absorption processes between narrow, well-defined energy states because they lead to sharp line spectra. It is the high resolution spectroscopy of semiconductors in the near and far infrared region which has profitted extraordinarily from FTS. This review has been written with the nonspecialist in mind who knows basic science but not necessarily semiconductors. The simple introductory explanations in the following chapters are not meant to be read by experts in the field! They are, however, useful in understanding the sections which follow.

2. Electronic Excitations

2.1 Elemental Shallow Donors and Acceptors

Substitutional phosphorus in the Si diamond lattice may be regarded as the prototype of a shallow donor. The fifth valence electron of phosphorus is not required for bond formation with the four Si neighbors and it is bound with an energy of only 45.59 meV to the positive phosphorus core [1]. In an analogous manner, aluminum in a substitutional position forms a shallow acceptor binding a hole with an energy of 70.18 meV. The hole is created because the aluminum impurity with only three valence electrons completes the fourth bond by "borrowing" an electron from the valence band. The effective mass theory developed by Kittel and Mitchell and by Kohn and Luttinger in the mid-1950's [2,3] explains the shallow impurities in terms of hydrogen-like systems imbedded in a continuous medium with the relative dielectric constant ε_r. The well-known equation for the groundstate binding energy of the hydrogen atom is modified by introducing the relative dielectric constant ε_r and by replacing free electron mass with the effective mass m*. The binding energy E of a "hydrogenic" system is:

$$E = \frac{e^4 m^*}{2\varepsilon_r^2 \varepsilon_o^2 h^2} = 13.6 \text{ eV} \frac{m^*}{\varepsilon_r^2 m_o} \tag{1}$$

and the Bohr radius becomes:

$$r = \frac{\varepsilon_r \varepsilon_o h^2}{e^2 m^*} \tag{2}$$

The constants are: the charge of the electron $e = 1.6 \times 10^{-19}$As, Planck's constant/$2\pi = 1.05 \times 10^{-34}$Js and the permittivity of vacuum $\varepsilon_o = 8.85 \times 10^{-16}$Fm^{-1}. The typical relative dielectric constant ε_r of a semiconductor has a value > 10 which leads to a reduction of $E_{hydrogen}$ by more than two orders of magnitude. The effective mass, which needs to be appropriately averaged over all $\vec{k}$-space directions, can be smaller than the free electron mass by factors of more than 3, further reducing E. The binding energies of hydrogenic donors and acceptors in Si, Ge, and GaAs range from a few meV to ~ 100 meV or in wave numbers from about 10 cm^{-1} to 1000 cm^{-1}. Optical processes in shallow hydrogenic centers therefore take place in the far infrared region of the electromagentic spectrum. A comprehensive modern review of the hydrogen analogue in semiconductors, the shallow donors and acceptors, has been written by Ramdas and Rodriguez [1]. Here I simply summarize those major features of shallow levels which are important for the understanding of impurity spectra.

Shallow donors and acceptors exhibit, in addition to their groundstates, series of bound excited states. The band structure of the host crystal produces a number of pronounced effects on the energy spacings between the various states and on their symmetries.

Donors in Si have a sixfold set of 1s states due to the location of the six conduction band minima along the <100> crystal momentum space axes ($\vec{k}$-space). The states are grouped into a 1s singlet (A_1), a 1s doublet (E) and a 1s triplet (T_2). The singlet 1s (A_1) is most sensitive to the potential at the core of the impurity and is typically the lowest lying state, i.e., the ground state. The 1s(E) and (T_2) states are less sensitive to the impurity core potential and they lie typically close together near the energy predicted by the effective mass theory. The situation for donors in Ge is slightly different because the four conduction band minima are located along the <111> axes in $\vec{k}$-space leading to a 1s(A_1) and 1s(T_2) set of states.

Again, in analogy to hydrogen one finds s-, p-, d-, etc. bound excited states associated with hydrogenic donors. The particular band structures of Si and Ge cause the p-states to split into a p_o singlet state (magnetic quantum number m = 0) and a $p_\pm$ doublet state (m = ±1). The first

accurate calculations of the groundstate and bound excited state energies were performed by Faulkner [4]. Recent calculations by Broeckx, et al. [5] are accurate to within ± 0.001 meV for more than ten states. An impressive example of the Lyman transitions $1s(A_1) \rightarrow np$, $n = 2,3,4$ etc. of phosphorus donors in silicon is shown in Fig. 1 [6]. The IR absorption measurements were performed at a temperature close to 4 K where all the bound electrons reside in the $1s(A_1)$ ground state. Measurements at higher temperatures would reveal transitions from the other 1s states because of thermal population from the ground state.

The donors in this particular Si crystal have been introduced using a unique doping technique called neutron transmutation doping (NTD) [7]. Some of the ^{30}Si nuclei, abundant with 3.1 atomic % in the undoped crystal, were allowed to capture thermal neutrons in a nuclear reactor. Phosphorus is produced according to the following β-decay reaction with a half life of 2.6 hours:

$$^{30}_{14}Si + n \rightarrow ^{31}_{14}Si \rightarrow ^{31}_{15}P + e^- + \bar{\nu}_e$$

The phosphorus atoms are shallow donors only when they reside in substitutional lattice locations. Recoil from the β-decay or radiation damage caused by fast neutrons leaves many phosphorus atoms in non-substitutional positions. Moving all the phosphorus into the proper lattice locations is achieved by thermal annealing which also removes fast neutron damage. The beta particle (e^-) and the electronic antineutrino ($\bar{\nu}_e$) do not leave any permanent changes in the crystal. One of the beneficial aspects of NTD is the ideal doping uniformity which simply cannot be achieved by any other doping technique involving a phase transformation (e.g. growth of a crystal from a doped melt). A further advantage is the control over the starting material before doping. One typically uses high-purity Si which can be thoroughly characterized with electrical and optical techniques before doping.

Let us now turn our attention to shallow acceptors which differ in several significant ways from donors. The differences are associated with the band-structure. Shallow acceptor states are situated near the top of the valence band which is located in diamond and zincblende semiconductors at the center

of the Brioullin zone ($\vec{k} = 0$). There are two bands--the light and the heavy hole bands--which are degenerate at $\vec{k} = 0$. The twofold band degeneracy together with the two spin orientations lead to acceptor states with Γ_8 symmetry, transforming according to operations of the double group T_d.

An additional band, the split-off band, lies below the top of the heavy/light hole bands by an energy difference called the spin-orbit splitting energy. We omit discussion of the effect of this band on acceptor states, though it clearly has an influence in the case of silicon, where the split-off energy of 42.8 meV is of the same order of magnitude as the shallow acceptor binding energies. In germanium the split-off energy is 300 meV, large enough to make the effects of this band undetectable.

Figure 2 shows the bound excited state spectrum of substitutional Al and B acceptors in pure germanium. Two series of lines originating from a hydrogen-carbon acceptor complex are also seen. The lines are labeled according to the scheme introduced by Jones and Fisher [8]. At the time of these experimental studies there existed no theoretical calculations which would have allowed them to label the lines with the correct symmetry and quantum numbers. In the meantime, detailed calculations have been performed by Baldereschi and Lipari [9]. These elaborate calculations were undertaken after shallow acceptor spectra, recorded with ultra-pure germanium [10-13], had revealed many more lines with much smaller width than previously reported.

An interesting and often very useful feature of both acceptor and donor spectra is the experimental finding that the energy differences between a given pair of bound excited states is a constant for all group III acceptors and all group V donors respectively. This shows that all the non-s-like excited states, the ones observed with single photon-induced transition between the s-like ground state to a non-s-like excited state, are insensitive to the central cell potential near the impurity which creates the shallow state. This insensitivity is readily understood on the basis of the nature of the wavefunctions of the p, d, etc. excited states which vanish at the impurity core. It further means that the central cell potential is truly localized, limited to less than a lattice constant. The consequence of this experimental finding is that each acceptor (donor) spectrum exhibits a series of

lines with identical spacings but shifted to higher or lower energies depending on the location of the ground state relative to the band edge (Fig. 3). This great redundancy is most useful during the discovery of novel shallow centers. So far, every one of the more than twenty novel shallow centers found in Ge and Si have shown a complete set of excited state lines. Haller [14] has compiled most of the known shallow acceptors and donors in Ge.

2.2 Photothermal Ionization Spectroscopy (PTIS) with Ultra-Pure Crystals

The development of ultra-pure Ge for nuclear radiation detectors has resulted in a series of discoveries of hitherto unknown shallow donors and acceptors which are not associated with single elemental group III or group V impurities. These centers are present at relatively low concentrations, ranging typically from 10^{10} cm^{-3} to 10^{11} cm^{-3}. These very low concentrations are the main reason why the centers had not been discovered earlier in doped Ge. Another reason, one on which I will elaborate later, is related to the special crystal growth conditions which are used in the growth of ultra-pure material. Before discussing the novel impurity centers, it is worthwhile to briefly describe the experimental method which is used to perform spectroscopy at such small concentrations of shallow acceptors and donors. The usual absorption spectroscopy ceases to work around concentrations of 10^{12} cm^{-3} because the linear absorption coefficient becomes too small to obtain signal-to-noise ratios larger than unity. Electrical measurements of shallow levels, based on conductivity or Hall effect, are sensitive to lower concentrations than optical absorption, but they typically do not exhibit spectroscopic character.

At sufficiently low temperatures, extrinsic impurity-caused conductivity is the dominant conduction mechanism. It decreases exponentially with temperature because the electrons (holes) become bound to the donor (acceptor) ions. In this "frozen-out" state in which impurities are neutral, light can be used to photoionize the bound electrons (holes). The sharp rise in conductivity at the photon energy corresponding to the binding energy is called photoconductive onset and is schematically shown in Fig. 4a. Lifshits and Nad [22] discovered discrete photoconductivity peaks below the photoconductive onset (Fig. 4b, c) when they performed spectrally resolved photoconductivity

experiments with lightly doped Ge samples at temperatures between 6 K and 10 K. They correctly interpreted this phenomenon in terms of a two-step ionization process which we have named photothermal ionization (PTI). The PTI process is shown schematically in Fig. 5. The usual dipole transitions between the 1s ground state and the bound excited states caused by photon absorption are followed by thermal ionization from the bound excited states to the continuum. The probability for the thermal ionization step to occur increases with decreasing energy difference between the bound excited state and the band edge and rises sharply with temperature because of the rapid increase in the phonon population. PTI has become a very powerful spectroscopy technique because it is both sensitive and spectroscopic. The early measurements were performed with 1 m^2 size grating spectrometers. Very quickly FTS was exclusively used for photothermal ionization spectroscopy (PTIS). Soon it was recognized that the signal-to-noise ratio for PTIS does not depend to first order on the impurity concentration in the crystal under investigation [23]. Ge samples with a total amount of 10^8 Al acceptors produce spectra (Fig. 2) with signal-to-noise ratios of the largest peaks > 100. Indeed we have determined shallow impurity species down to 10^5 total impurities in some very pure samples. The PTI process has been analyzed quantitatively for a number of different impurity/crystal combinations [24,25].

2.3 Transition Line Widths of Shallow Levels

Because donor and acceptor impurities have very large Bohr radii (10 - 100 Å) and are imbedded in nonperfect solids, their wavefunctions experience a variety of disturbances. The large spatial extent of the wavefunctions of the ground and bound excited states leads to interactions with neighboring impurities at very low impurity concentrations. It is, therefore, not surprising that the early shallow level spectra did not exhibit very sharp lines. In recent years, however, extremely pure crystals with very small dislocation densities and other native defect concentrations have been grown [15]. In addition, we discovered a shallow donor complex in Ge which is insensitive to stress. In combination, these advances have led to spectra with lines as narrow as a few μeV (0.01 cm^{-1}), fully utilizing the capabilities of today's FTS instrumentation.

The improvements in semiconductor crystal quality and the capabilities of commercial FTS instrumentation appear to have progressed at a similar pace. The best commercial instruments possess spectral resolutions which meet the most taxing experimental demands.

What is the ultimate line width of a 1s to np (Lyman series) transition? Barrie and Nishikawa [16,17] proposed more than twenty years ago that final state interactions are the main cause for line broadening. Kane [18] had shown earlier that phonon emission or absorption-assisted transitions contribute to a very broad background. The lines are due to no-phonon transitions. The final state interacts with neighboring states via low energy longitudinal acoustic phonons. This broadening mechanism, sometimes called "lifetime" broadening, had not been observed experimentally until recently because the crystals were simply not perfect enough. Jagannath, et al. [6] and later Pajot, et al. [19] obtained the highest resolution spectra of elemental donors in Si. They observed line widths of the order of 15 μeV (0.12 cm^{-1}). Because all the lines showed the same width in a given sample, they postulated that ground state broadening must be the major contributor to the line width. Navarro, et al. [20] used magnetic tuning of several 1s-np transitions of a stress insensitive donor complex in Ge to measure line widths with a CO_2 laser pumped alcohol laser. They found lines as narrow as 6 μeV. Adapting Barrie and Nishikawa's calculations to the case of donors in Ge, they estimated a final state interaction contribution of a few μeV. Taking into account the simplifications made by Barrier and Nishikawa in their theory, it is impressive to see how well the experimental results agree with the theoretical predictions. It is likely that these values of line width are fundamental and that they will not be substantially decreased in the near future.

Pajot and Stoneham [21] have recently used the very high resolution capability of modern FTS instrumentation to determine spectroscopically the lattice distortions introduced by non-isocoric impurities in Si. Based on extremely small donor-impurity-species-related changes in the energy differences between equivalent excited states, they conclude that the volume difference between an impurity and a Si host atom causes long range lattice distortions which are different from the central cell effects. These long range

distortions affect p-like states which have a node at the origin of the impurity and are, as mentioned earlier, insensitive to the central cell potential.

2.4 Novel Centers and Impurity Complexes in Ultra-Pure Ge

Hall [26] discovered a shallow acceptor at a concentration close to 2 x 10^{11} cm^{-3} after rapidly quenching ultra-pure Ge specimens from temperatures around 425°C. Annealing the crystal at a temperature between 25°C and 80°C annihilated the acceptor and led to the formation of a shallow donor also at a concentration close to 2 x 10^{11} cm^{-3}. Haller [27] showed by substituting the hydrogen crystal growth atmosphere with a pure deuterium atmosphere that both the rapid quench acceptor as well as the donor experience a small shift in their ground state energies as a result of this isotope shift. This was the first direct proof of the presence of hydrogen in these centers. Only FTS allowed the detection of the acceptor shift of 21 μeV (0.17 cm^{-1}) and the donor shift of 51 μeV (0.44 cm^{-1}). Experiments with growth in mixed atmospheres (H_2 and D_2) further revealed that only one hydrogen isotope is present in these centers [11]. Figure 6 displays two spectra--one of a sample from a p-type Ge crystal grown in a H_2 atmosphere, the other of a sample from a n-type Ge crystal grown in a D_2 atmosphere. In both spectra, we can observe line series from donors and acceptors though with opposite signs. This has been made possible by illuminating the crystals with above bandgap light ($h\nu > E_{gap}$) which generates free electrons and holes. These in turn are captured by the donors and acceptors respectively, yielding them available to PTIS. The isotope shift between the hydrogen-related donor spectra is most easily seen in the displacement of the $1s - 2p_{\pm}$ lines of the rapid quenching donor. The donor ground state shift ΔE_{gs} is 51 μeV. The positions of the lines of the elemental acceptors Al and B and the donor P coincide perfectly in both spectra, producing an independent and highly redundant calibration of the two energy axes. The reasons for the positive and negative lines lie in a subtle balance of free and bound hole and electron concentrations respectively. Quantitative models have been developed for PTIS under band edge illumination [24,28].

Further information about the nature of the rapid quench centers was gained from the strong correlation of the concentration of the two centers

with the crystal growth crucible material. Ultra-pure Ge crystals are grown by the Czochralski technique from melts contained in synthetic silica crucibles [15]. The Ge melt slowly reduces the silica, leading to free oxygen and silicon in the melt which in turn enter the single crystal at concentrations of approximately 10^{14} cm^{-3}. Isolated silicon in a substitutional position in the Ge lattice does not produce any electronic levels in the bandgap. Oxygen in a bond centered position between two Ge host atoms is also electronically inactive. The hydrogen growth atmosphere results in a hydrogen concentration in the single crystals of approximately 10^{14} cm^{-3}. Experiments with a very large number of ultra-pure Ge crystals grown under a variety of conditions have shown that the rapid quench donor and acceptor are always present in crystals grown in a hydrogen atmosphere from a melt contained in a silica crucible. The centers are, however, not present in crystals grown under alternate conditions. This leads us to conclude that the two new centers contain silicon and oxygen. Doping with an excess of silicon suppresses the donor formation while increasing the acceptor concentration by a factor of ~ 3 which means that the donor consists of oxygen and hydrogen--D(H,O). The acceptor, on the other hand, contains hydrogen and silicon--A(H,Si). In graphite-crucible-grown crystals, an acceptor A(H,C), the analog of A(H,Si), was found.

In order to reveal the structure of these centers, various PTIS experiments were performed using external perturbations of the crystal and variable temperature. I will review here only the major results, making extensive use of published results.

The first surprising result which we obtained with A(H,Si) and A(H,C) was the discovery of a split 1s state. PTIS revealed a second hydrogenic set of lines increasing in strength with increasing sample temperature. Under uniaxial stress the lines of both series did not split as expected for shallow acceptors [1]. This unexpected behavior meant that the shallow acceptors could not be explained with effective mass theory and the band structure near $\vec{k} = 0$ alone, but that an extra degree of freedom was required to model these centers. Such a model was developed by Falicov [29]. It is based on centers with substitutional Si or C and interstitial hydrogen tunneling between four equivalent real space positions [30].

More recently the tunneling hydrogen model has been successfully used by Muro and Sievers [31] to explain spectra of shallow acceptor complexes in Si consisting of substitutional beryllium double acceptors binding one hydrogen atom. The proton may simplistically be viewed as the replacement of one of the two holes bound to Be.

Very high resolution studies of A(H,Si) and A(H,C) by Kahn, et al. [32] yielded results which were characteristic for the uniaxial stress behavior of a trigonal center. Each of the hydrogenic lines splits under [111] uniaxial stress in a 3:1 intensity ratio and a 3:1 energy shift ratio away from the zero stress position. Figure 7 shows the D-lines of A(H,Si), Al, and B at three different values of [111] stress. At the lowest stress, the D-lines of B and Al are symmetrically split while the D-lines of the two series of A(H,Si) designated D[1] and D[2] only show slight asymmetries. At the intermediate stress value, the 3:1 intensity ratio of $D_1[2]$ and $D_2[2]$ and the 1:3 energy shift ratio is clearly visible. At the highest stress value, the line splittings are large and several lines overlap one another. Based on the new high-resolution results, tunneling of hydrogen is not required any longer to explain the experimental findings. An internal stress dipole parallel to [111] and extending only over the central cell region splits the fourfold degenerate 1s-like ground state but leaves the p-like excited states unchanged. Additional external uniaxial stress leads to orientational splitting, i.e., three out of four A(H,Si) centers have their built-in dipole not oriented along the external stress while one out of four does have the internal dipole parallel to the applied stress. The internal stress dipole model fully explains the behavior of all the A(H,Si) lines under uniaxial stress in all the major crystal orientations. The physical meaning of the stress dipole is, at this point in time, not fully understood. It is essentially a mathematical device which leads to a Hamiltonian with the appropriate perturbation. An electrical dipole caused by charge separation between the Si and the H atom would lead to the same model.

Two further centers which have been generated in hydrogen-atmosphere-grown Ge crystals are related to the double acceptors Be and Zn [ ]. We call these centers A(Be,H) and A(Zn,H). We discovered these impurity complexes while studying Be- and Zn-doped Ge crystals which are used for far infrared

detector applications [34,35]. The acceptor A(Be,H) has two 1s state components leading to two hydrogenic line series. A(Zn,H) shows only one set of lines because the split-off 1s state is too far removed to become thermally populated at the highest possible measurement temperatures. Under uniaxial stress in the [111] direction, we again observe behavior characteristic of a center with trigonal symmetry. In this case, however, the components of the centers oriented along the stress move closer to one another while the lines of the centers off the stress direction push apart. This is precisely the opposite behavior observed with A(H,Si) and A(H,C).

The difference between the two pairs of centers may be caused by the role hydrogen plays in the two cases. Shallow acceptors have a negatively charged core binding a positive hole. In order for the A(H,Si) or the A(H,C) cores to be negatively charged, the hydrogen must bind its second 1s electron assuming a H^- state. In the case of A(Be,H) or A(Zn,H), we already mentioned earlier that the proton replaces one of the holes, i.e., hydrogen assumes the H^+ state. If we assume that in all four cases hydrogen is located along an antibonding position, we obtain electric dipoles of opposite orientation for A(H,Si)/A(H,C) and A(Be,H)/A(Zn,H). This in turn would explain the opposite splitting of the ground states of the two impurity complex pairs. The opposite charge state of hydrogen in the two pairs of complexes is reflected in the ordering of the symbols in the parentheses.

We have so far discussed four hydrogen-related centers. There are many more centers involving one or more hydrogen atoms and a second impurity. Many of these centers are not electrically active because hydrogen fully passivates the other impurity. The best known case is hydrogen-passivated boron in silicon [36]. Unfortunately, such complexes cannot be studied with PTIS.

The only known center which is electrically active and contains more than one hydrogen atom is the dihydrogen-copper acceptor [$A(Cu,H_2)$] in Ge. Kahn, et al. [37] unambiguously demonstrated that a shallow acceptor $A(Cu,H_2)$ exists by using deuterium and tritium substitutions. In the $A(Cu,H_2)$ center, hydrogen performs tunneling while in all the centers with at least one heavy hydrogen isotope only librational motion occurs. The spectra of the

three centers A(Cu,H_2), A(Cu,H,D), and A(Cu,D_2) are shown in Fig. 8. The difference in character between the spectrum of A(Cu,H_2) and the other two spectra is striking. A very large isotope shift, in large part caused by the different motion of the hydrogen isotopes, further supports the idea that the hydrogen-containing center has an additional degree of freedom compared to the other two centers which display very simple spectra. The H_2-containing center displays many hydrogenic series originating in a rich 1s-state manifold. The proximity of the various s-states leads to observable thermal population even at low temperatures.

3. Local Vibrational Modes

In Section 2, we discussed the interaction of photons with the electrons in a solid. Now we will review the interactions between photons and atoms (ions). As in the previous section, we will concentrate on those interactions which lead to sharp line spectra.

Any discussion of the optical activity of solids in the infrared has to begin with a brief review of the vibrational modes of a perfect crystalline solid. The description of a solid with the popular ball and spring model was first used in 1686 by Newton [38]. In a recent review by Barker and Sievers [39], a chain of balls and springs, closed in itself in order to circumvent the boundary problem, has been used to arrive at the vibrational spectrum of a solid. The four types of vibrational frequencies which are found in crystalline solids are: longitudinal acoustic (ω_{LA}) and optical modes (ω_{LO}), transverse acoustic (ω_{TA}) and optical modes (ω_{TO}). The quantized vibrations are called phonons. The interaction of photons and the partially ionic solid GaAs is very pronounced in the optical phonon energy range. The famous "Reststrahlen" band (residual rays band) [40] in which the crystal reflects a very large fraction of the incident photons is the phonon frequency range between ω_{LO} and ω_{TO} (Fig. 9 [41]). Lattice vibrations, however, are not very exciting for the high resolution spectroscopist because they lead to broad bands. A very different situation arises when impurities with a mass smaller than that of the host atoms are introduced and investigated. Barker and Sievers' article contains detailed information on vibrational modes introduced by a large number of impurities in many solids. Simply stated, light

impurities vibrate at significantly higher frequencies than the lattice vibrations. They are strongly coupled to their immediate neighbors but are largely decoupled from the rest of the lattice and generate spatially localized vibrations which appear as sharp absorption lines at energies well above the lattice absorption bands. Cooling of the crystal leads to sharper vibrational modes because the lattice phonon density decreases.

Depending on the local atomic configuration around a certain impurity, one observes more than one absorption line. A beautiful example is oxygen in silicon and germanium. The far and near IR absorption of oxygen in silicon has been studied by numerous researchers. One of the most extensive studies was publisehd by Bosomworth, et al. [42]. Based on the generally accepted model of isolated oxygen assuming bond-centered interstitial positions forming a Si_2O molecule, the authors were able to identify most of the oxygen-related vibrational modes. The strongest absorption features are observed in the so-called ν_3 band near a wavelength of 9 μm. These features were assigned to antisymmetric stretch vibrations. The four lines in the ν_3 band arise from the low frequency symmetric banding vibrations grouped together in the ν_2 band which superimposes the ν_3 band. The lines in the ν_2 band lie in the 30 to 50 cm^{-1} region. The vibrations are described by a harmonic potential which ignores any interaction between Si_2O and the lattice. Figure 10 summarizes the various vibrational states of bond-centered interstitial oxygen in silicon. Using isotopic substitution and uniaxial stress, the microscopic nature of the Si_2O molecule could be determined and all the vibrational modes could be assigned. The angle between the two oxygen bonds is found to be 162°. For further details of this important center in silicon, the reader is encouraged to consult the original literature.

As a simple rule for the linewidths of vibrational mode transitions, we can state that the further an impurity mode is removed from lattice modes, the less the mode couples to the lattice and the sharper it will be. This fact has been most beautifully demonstrated by Pajot and Clauws [43] who investigated the oxygen vibrational mode spectrum in germanium. Germanium consists of five isotopes, three of which are present with similar abundance while two

constitute less than 10% each. Oxygen resides, as in silicon, in a bond-centered interstitial site forming a Ge_2O molecule. The five Ge isotopes give rise to 15 different neighboring pair combinations, i.e., 15 isotope-shifted lines in the ν_3 antisymmetric stretch band. Superposition with the ν_2 low frequency symmetric bending band leads to three lines in the ν_3 band, each experiencing small shifts due to the 15 possible isotope combinations. Of the total of 45 lines, 33 have been resolved! Figure 11 reproduces Pajot and Clauws' spectrum of the ν_3 band of oxygen in germanium recorded at 6 K. The oxygen concentration in the sample was 5×10^{16} cm^{-3} and the spectrum was recorded with FTS at a resolution of 0.03 cm^{-1}. The narrowest line has a width of 0.035 cm^{-1} ($\sim$ 4 μeV) which is to our knowledge, the narrowest line for vibrational and electronic transitions in semiconductors.

In the third example of local mode vibration spectroscopy in crystalline semiconductors, we consider carbon in gallium arsenide. Carbon preferentially occupies the arsenic site (C_{As}). In this position, it forms a shallow acceptor because it has one valence electron less than the arsenic atom it replaces. The vibrational modes of this impurity have been experimentally studied by Theis, et al. [44] and modeled by Leigh and Newman using an XY_4 molecule [45]. Herzberg [46] has derived nine possible modes for such molecules. The LVM spectrum of carbon displays only five lines because some of the lines are accidentally superimposed. Figure 12a shows the spectrum of ionized carbon in GaAs. Shanabrook, et al. [47] have shown that this spectrum changes significantly when the carbon acceptor binds a hole (Fig. 12b and c). It is, in fact, possible to deconvolute spectra and find the ratio of charged to neutral carbon acceptors. This has been used by Walukiewicz, et al. [48] in a recent study of the distribution of native defects and residual impurities in as-grown, large GaAs bulk crystals. Such crystals typically contain three groups of important centers: shallow acceptors caused predominantly by carbon, shallow donors, and a deep double donor called EL2 which is due to a native defect. This donor has the unusual property in that it can be optically quenched, i.e., its energy level can be moved out of the bandgap with optical pumping. Measuring spatially resolved the ratio of ionized to neutral carbon for both the quenched and unquenched crystal, and the concentration of

EL2 with optical absorption, Walukiewicz, et al. [48] have been able to find the spatial distribution of all three groups of centers in bulk GaAs crystals. Such results are of importance for the GaAs technologist who wants to build GaAs integrated circuits consisting of large numbers of metal semiconductor field effect transistors (MESFETs). The characteristics of MESFETs strongly depend on the local concentrations of residual impurities and native defects.

4. Discussion

I hope the examples cited in the foregoing text amply demonstrate the progress in semiconductor science and technology which has been made possible through infrared FTS studies. Regarding spectral resolution, modern high performance instruments are capable of reproducing the true line shapes of even the sharpest lines in semiconductor spectra. There are, however, other challenges lying ahead of us. With electronic device geometries becoming progressively smaller, one wishes to analyze ever smaller semiconductor sample volumes. This will require advanced optics and detectors working at the photon noise limit. New applications for FTS now also include photoluminescence (PL) in which a semiconductor sample which is excited by a strong laser acts as the light source in an interferometer. In exploratory PL studies, FTS provides a quick and efficient means of finding new spectral features. The stability of modern lasers is sufficiently good to yield low noise PL FTS results. I am convinced that FTS will in the future not only be of benefit to semiconductor science but that advances in semiconductor technology will further FTS. The appetite of FTS for faster computers with more digits and larger memory capacity will hardly subside!

Acknowledgments

I am indebted to many people whose work I have used in this review. The use of P. L. Richards' IR facilities, the work of my former students, R. E. McMurray, Jr. and J. M. Kahn, and the theoretical input from L. M. Falicov have had the greatest impact in the discovery and understanding of the novel centers in Ge. A. K. Ramdas and N. M. Haegel gave important advice for improving this manuscript.

This work was supported in part by the U.S. Dept. of Energy under Contract No. DE-AC03-76SF00098, and in part by the U.S. National Science Foundation under Contract No. DMR-8502502.

References

[1] A. K. Ramdas, S. Rodriguez, Rept. on Prog. in Phys. 1981, 44, 1297.

[2] C. Kittel, A. H. Mitchell, Phys. Rev. 1954, 96, 1488.

[3] W. Kohn, J. M. Luttinger, Phys. Rev. 1955, 97, 869.

[4] R. A. Faulkner, Phys. Rev. 1969, 184, 713.

[5] J. Broeckx, P. Clauws, J. Vennik, J. Phys. C 1986, 19, 511.

[6] C. Jagannath, Z. W. Grabowski, A. K. Ramdas, Solid State Comm. 1979, 29, 355; see also: C. Jagannath, Z. W. Grabowski, A. K. Ramdas, Phys. Rev. B 1981, 23, 2082.

[7] See, for example, articles in Proc. of the Fourth Neutron Transmutation Doping Conference, ed. R. D. Larrabee, Plenum Press, New York and London, 1984.

[8] R. L. Jones, P. Fisher, J. Phys. Chem. Solids 1965, 26, 1125.

[9] A. Baldereschi, N. O. Lipari, Phys. Rev. B 1973, 8, 2697; Phys. Rev. B 1974, 9, 1525; and Proc. 13th Intl. Conf. Phys. Semiconductors, ed. F. G. Fumi, North Holland, 1976, p. 595.

[10] E. E. Haller, W. L. Hansen, Solid State Comm. 1974, 15, 687.

[11] E. E. Haller, W. L. Hansen, F. S. Goulding, Adv. in Phys. 1981, 30, 93.

[12] S. D. Seccombe, D. M. Korn, Solid State Comm. 1972, 11, 1539.

[13] M. S. Skolnik, L. Eaves, R. A. Stradling, J. C. Portal, S. Asknazy, Solid State Comm. 1974, 15, 1403.

[14] E. E. Haller, MRS Symposia Proc. 46, eds. N. M. Johnson, S. G. Bishop, G. D. Watkins, Mat. Res. Soc., Pittsburgh, PA, 1985, p. 495.

[15] W. L. Hansen, E. E. Haller, Mat. Res. Soc. Symp. Proc. 1983, 16, 1.

[16] R. Barrie, K. Nishikawa, Can. J. Phys. 1963, 41, 1823.

[17] K. Nishikawa, R. Barrie, Can. J. Phys. 1963, 41, 1135.

[18] E. O. Kane, Phys. Rev. 1960, 119, 40.

[19] B. Pajot, J. Kauppinen, R. Anttilla, Solid State. Comm. 1979, 31, 759.

[20] H. Navarro, E. E. Haller, F. Keilmann, to be published.

[21] B. Pajot, A. M. Stoneham, J. Phys. C: Solid State Phys. submitted for publication.

[22] T. M. Lifshits, F. Ya. Nad, Sov. Phys. Doklady 1965, 10, 532; for a review, see: Sh. M. Kogan, T. M. Lifshits, Phys. Stat. Sol. (a) 1977, 39, 11.

[23] Sh. M. Kogan, Sov. Phys. Semicon. 1973, 1, 828.

[24] G. Bambakidis, G. J. Brown, Phys. Rev. B 1986, 33, 8180.

[25] M. J. H. van de Steeg, H. W. H. M. Jongbloets, J. W. Gerritsen, P. Wyder, J. Appl. Phys. 1983, 54, 3464.

[26] R. H. Hall, IEEE Trans. Nucl. Sci. 1974, NS-21, 260; and Inst. Phys. Conf. Series 1975, 23 190.

[27] E. E. Haller, Phys. Rev. Lett. 1978, 40, 584.

[28] L. S. Darken, J. Appl. Phys. 1982, 53, 3754.

[29] L. M. Falicov, E. E. Haller, Solid State Comm. 1985, 53, 1121.

[30] E. E. Haller, B. Joos, L. M. Falicov, Phys. Rev. B 1980, 21, 4729.

[31] K. Muro, A. J. Sievers, Phys. Rev. Lett. 1986, 57, 897.

[32] J. M. Kahn, R. E. McMurray, Jr., E. E. Haller, L. M. Falicov, Phys. Rev. B in press.

[33] R. E. McMurray, Jr., N. M. Haegel, J. M. Kahn, E. E. Haller, Solid State Comm. 1987, 61, 27.

[34] N. M. Haegel, E. E. Haller, Infrared Phys. 1986, 26, No. 4, 247.

[35] N. M. Haegel, P. N. Luke, E. E. Haller, Intl. J. Infrared and Millimeter Waves 1983, 4, No. 6, 945.

[36] J. I. Pankove, D. E. Carlson, J. E. Berkeyheiser, R. O. Wance, Phys. Rev. Lett. 1983, 51, 2224.

[37] J. M. Kahn, L. M. Falicov, E. E. Haller, Phys. Rev. Lett. 1986, 57, 2077.

[38] I. S. Newton, Principia, Vol. II "The Motion of Bodies", Cambridge, 1686.

[39] A. S. Barker, A. J. Sievers, Rev. Mod. Phys. 1975, 47, Suppl. 2, 1.

[40] See for example: N. W. Ashcroft and N. D. Mermin, Solid State Physics, Saunders College, Holt, Rinehart and Winston, 1976.

[41] J. S. Blakemore, J. Appl. Phys. 1982, 53, R123.

[42] D. R. Bosomworth, W. Hayes, A. R. L. Spray, G. D. Watkins, Proc. Phys. Soc. London 1970, A317, 133.

[43] B. Pajot, P. Clauws, Proc. 18th Intl. Conf. Phys. Semiconductors ed. O. Engstroem, World Science Publishing, Singapore, 1986, p. 911.

[44] W. M. Theis, K. K. Bajaj, C. W. Litton, W. G. Spitzer, Appl. Phys. Lett. 1982, 44, 70.

[45] R. S. Leigh, R. C. Newman, J. Phys. C: Solid State Phys. 1982, 15, L 1045.

[46] G. Herzberg, Molecular Spectra and Molecular Structure II: Infrared and Raman Spectra of Polyatomic Molecules, Van Nostrand, Princeton, NJ, 1945.

[47] B. V. Shanabrook, W. J. Moore, T. A. Kennedy, P. P. Ruden, Phys. Rev. B 1984, 30, 3563.

[48] W. Walukiewicz, E. Bourret, W. F. Yau, R. E. McMurray, Jr., E. E. Haller, D. Bliss, Proc. Intl. Symp. on Defect Recognition and Image Porcessing in III-V Compounds, Elsevier Science Publishers, Amsterdam, in press.

Figure Captions

Fig. 1. Annealing of defects produced during the NTD process. The concentration of phosphorus generated is $\sim 2 \times 10^{15}$ cm^{-3}. (a) Before annealing. (b) After annealing for 2 h at 650°C. (c) After further annealing for 1 h at 800°C. The spectra were recorded using liquid helium as a coolant. The $2p_{\pm}$ line has been truncated because, with the thickness of the sample used, the transmission approaches zero at the peak. The instrumental resolution is 0.06 cm^{-1} without apodization. (Courtesy Ref. 6).

Fig. 2. PTI spectrum of a p-type ultrapure Ge sample obtained by Fourier transformation spectroscopy. The sample contains the acceptors B, Al and A(D,C), in a total concentration of 6×10^{10} cm^{-3}. The narrowest lines are 0.09 cm^{-1} = 11 μeV wide.

Fig. 3. The energy levels for the ground state and lowest-lying odd-parity excited states of Group III acceptors in Ge.

Fig. 4. Photothermal ionization spectroscopy (schematic). Typical spectra recorded at: (a) T = 0; (b) low T; (c) moderate T.

Fig. 5. The two-step ionization process which is the basis of PTIS.

Fig. 6. Isotope shift ΔE_{gs} in the ground-state binding energy of hydrogen-related donors.

Fig. 7. PTI spectra of the D transitions of $A(H,Si)_1$, $A(H,Si)_2$ and aluminum, under [111] uniaxial compression. In square brackets, the numbers "1" and "2" refer to $A(H,Si)_1$ and $A(H,Si)_2$, respectively.

Fig. 8. PTI spectra of the copper-dihydrogen acceptors that appear in samples which were grown under atmospheres of different hydrogen isotopes. (a) Pure H_2, showing the complex spectrum of A(CuH_2); (b) a 1:1 mixture of H_2 and D_2, showing A(CuH_2), A(CuHD) and A(CuD_2) in a 1:2:1 ratio; (c) nearly pure D_2, showing A(CuD_2) and a trace of A(CuHD).

Fig. 9. Normal incidence room temperature reflectance spectra for GaAs. (Courtesy Ref. 41).

Fig. 10. Energy level diagram for oxygen in silicon showing observed vibrational transitions in the near and far infrared. (Courtesy Ref. 42.)

Fig. 11. The ν_3 band of O_i in germanium (a) at 6 K, resolution: 0.03 cm^{-1}; (b) at 21 K, resolution: 0.05 cm^{-1}. (Courtesy Ref. 43).

Fig. 12. Dependence of the spectral form of the carbon LVM in GaAs on the carbon acceptor charge state. a) $[C^n]/[C^-] = 0$ (i.e., C is fully ionized); b) intermediate case; and c) $[C^n]/[C^-] = 4$. (Courtesy Ref. 47).

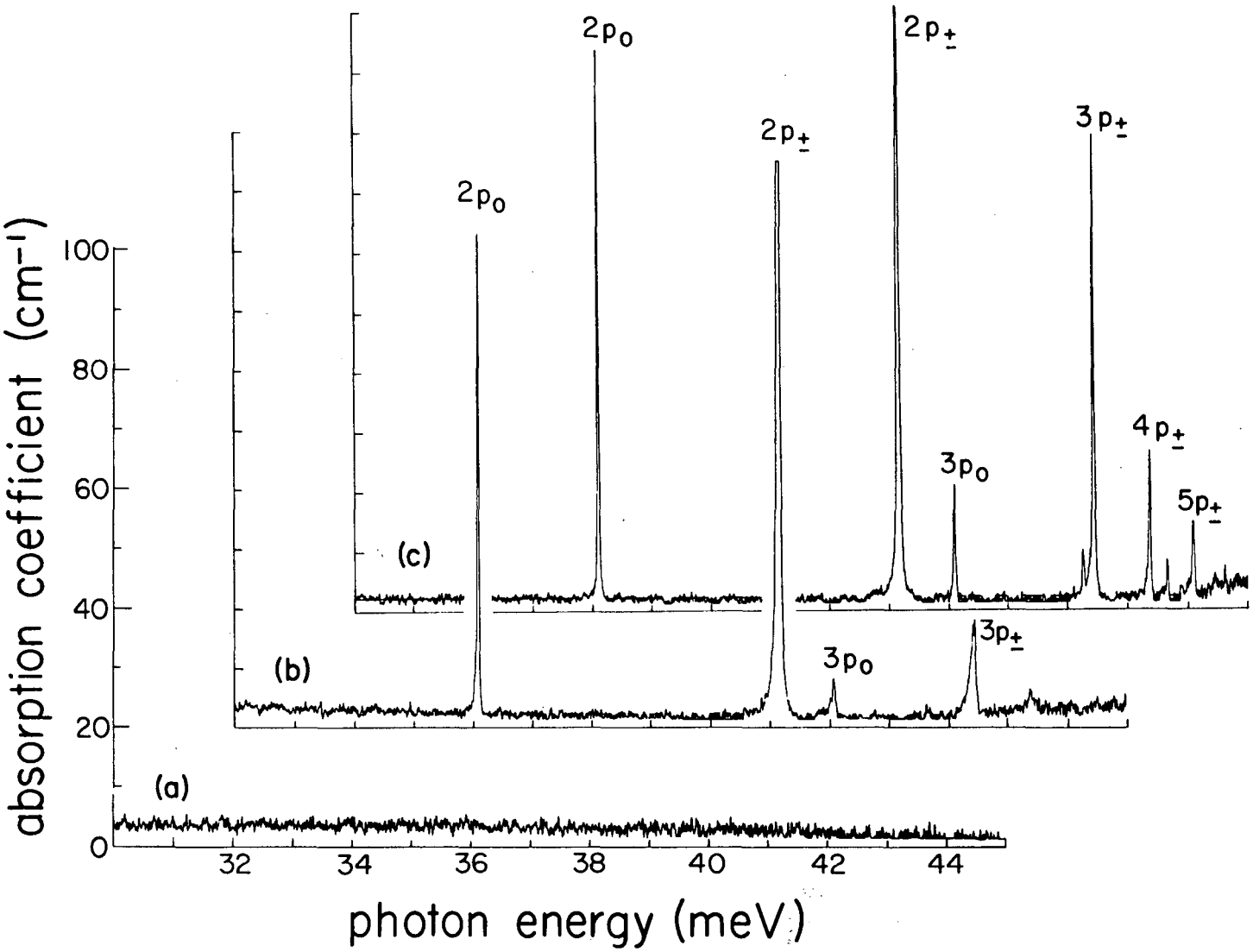

XBL 877-3351

Fig. 1.

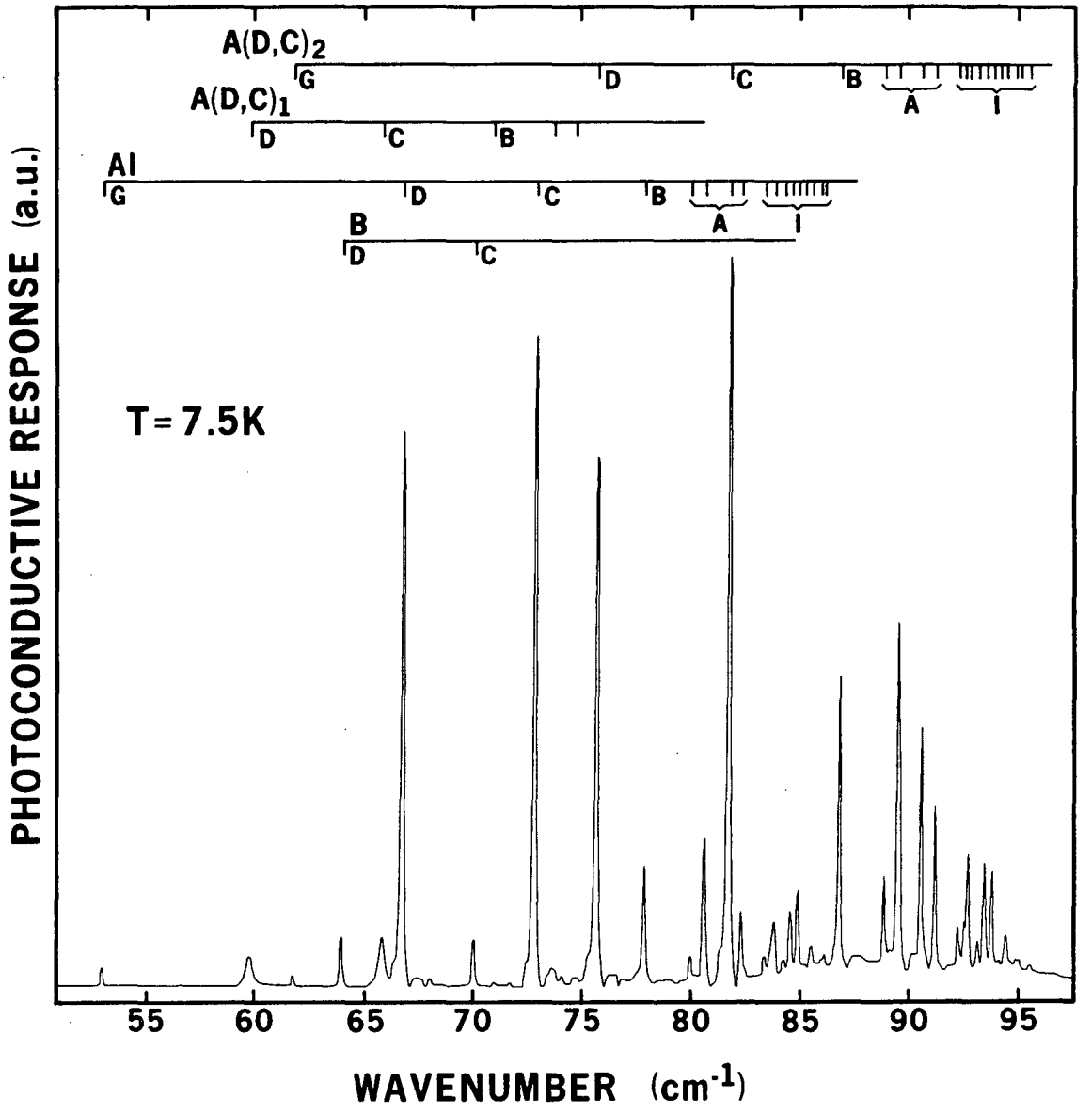

XBL 863-1160

Fig. 2.

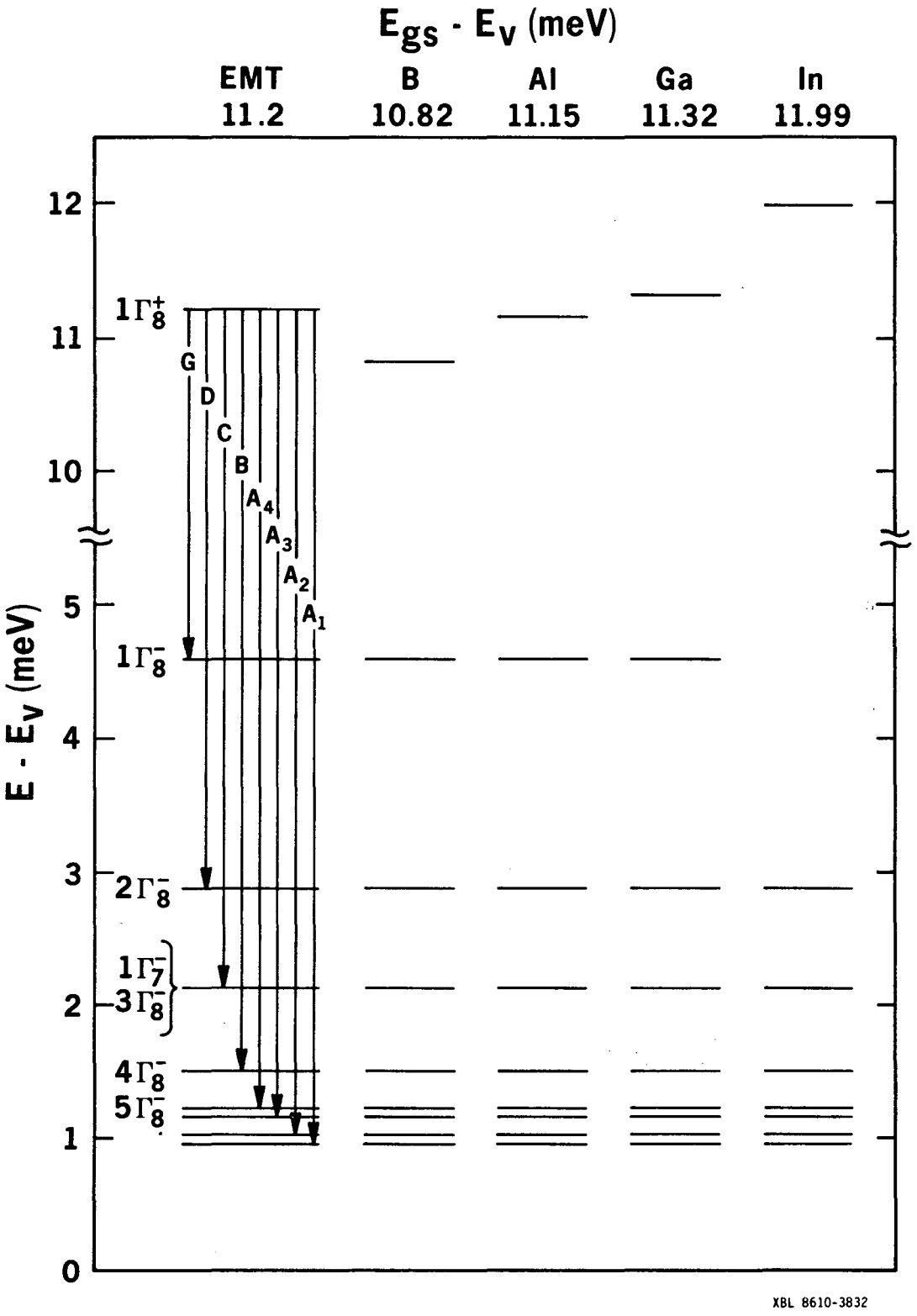
$E_{gs} - E_V$ (meV)
EMT 11.2
B 10.82
Al 11.15
Ga 11.32
In 11.99
$E - E_V$ (meV)
12
11
10
5
4
3
2
1
0
$1\Gamma_8^+$
$1\Gamma_8^-$
$2\Gamma_8^-$
$1\Gamma_7^-$
$3\Gamma_8^-$
$4\Gamma_8^-$
$5\Gamma_8^-$
G
D
C
B
A_4
A_3
A_2
A_1
XBL 8610-3832

Fig. 3.

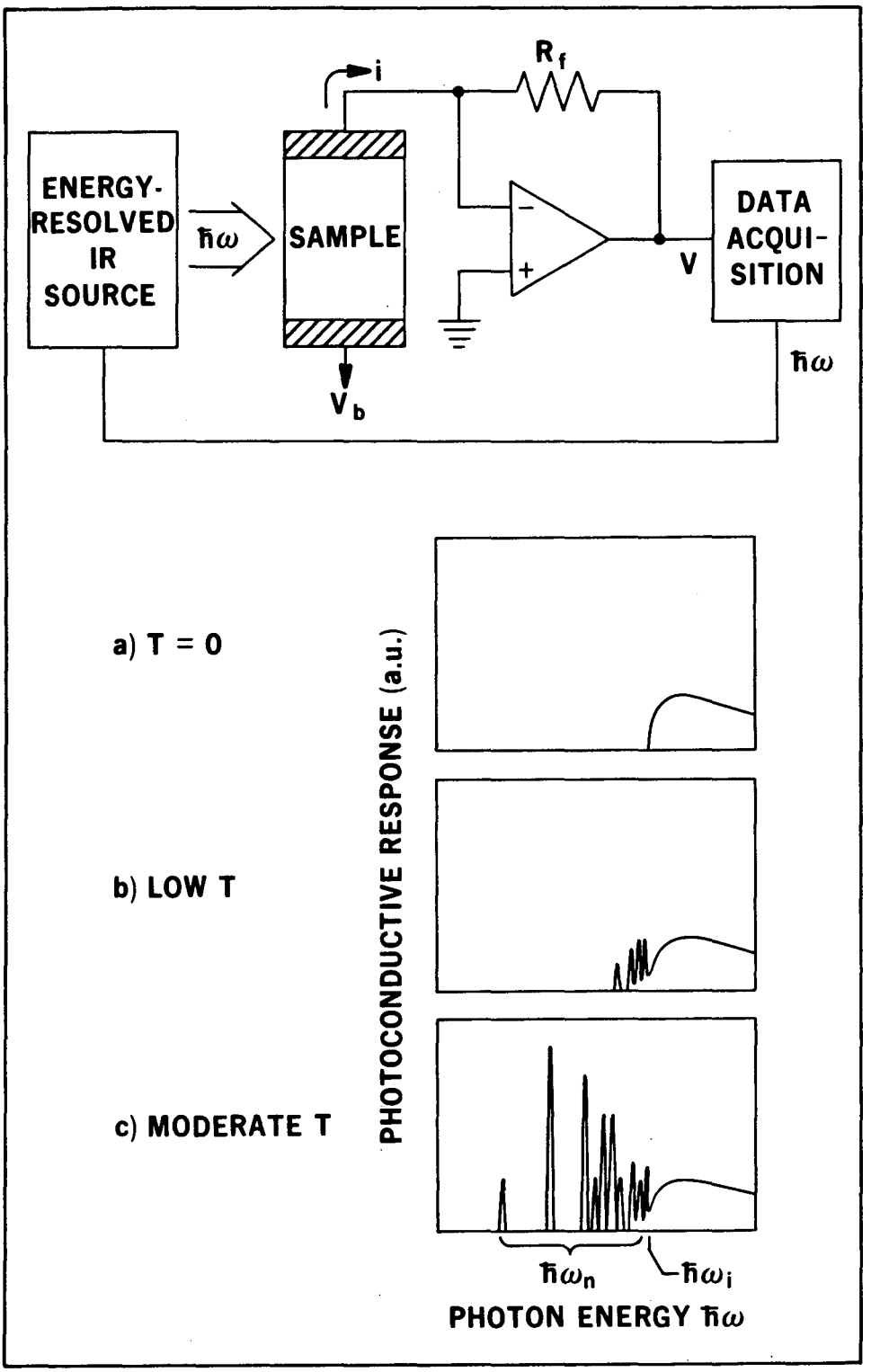

XBL 8610-3834

Fig. 4.

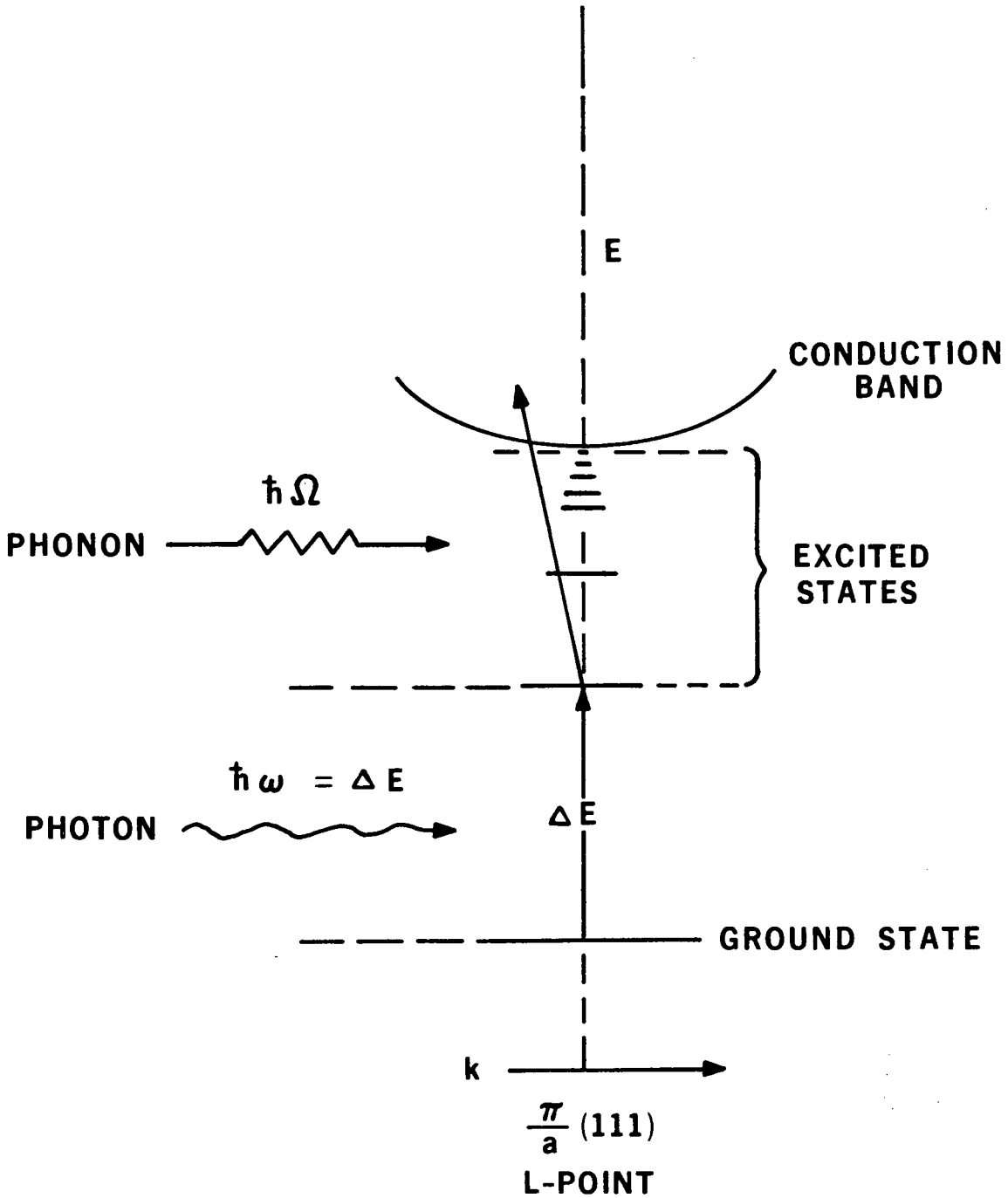
E
CONDUCTION BAND
ħΩ
PHONON
EXCITED STATES
ħω = ΔE
PHOTON
ΔE
GROUND STATE
k
π/a (111)
L-POINT
XBL 7411-8629

Fig. 5.

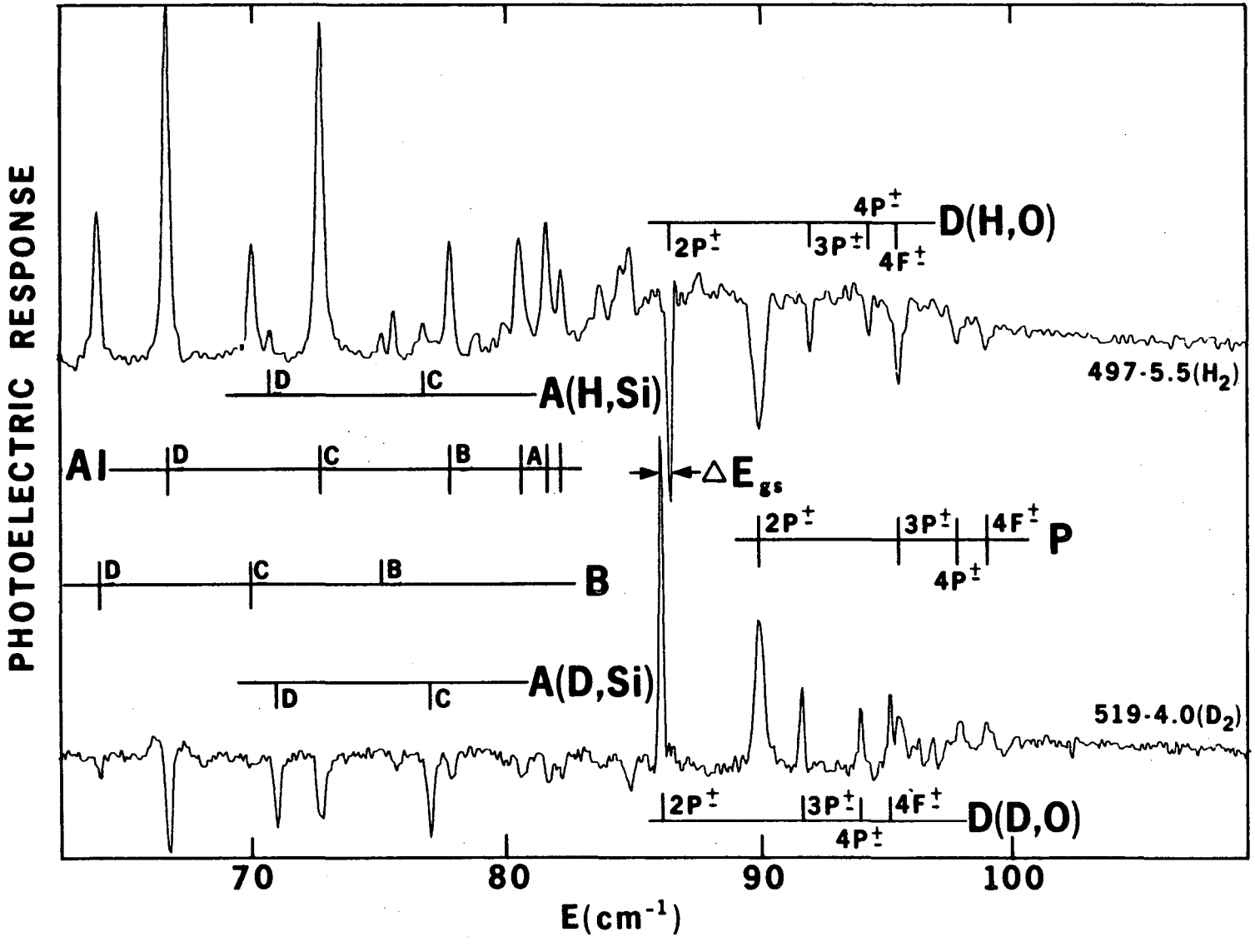
PHOTOELECTRIC RESPONSE
D(H,O)
2P±
3P±
4P±
4F±
497-5.5(H2)
A(H,Si)
D
C
Al
B
A
ΔEgs
P
519-4.0(D2)
A(D,Si)
D(D,O)
70
80
90
100
E(cm-1)

Fig. 6.

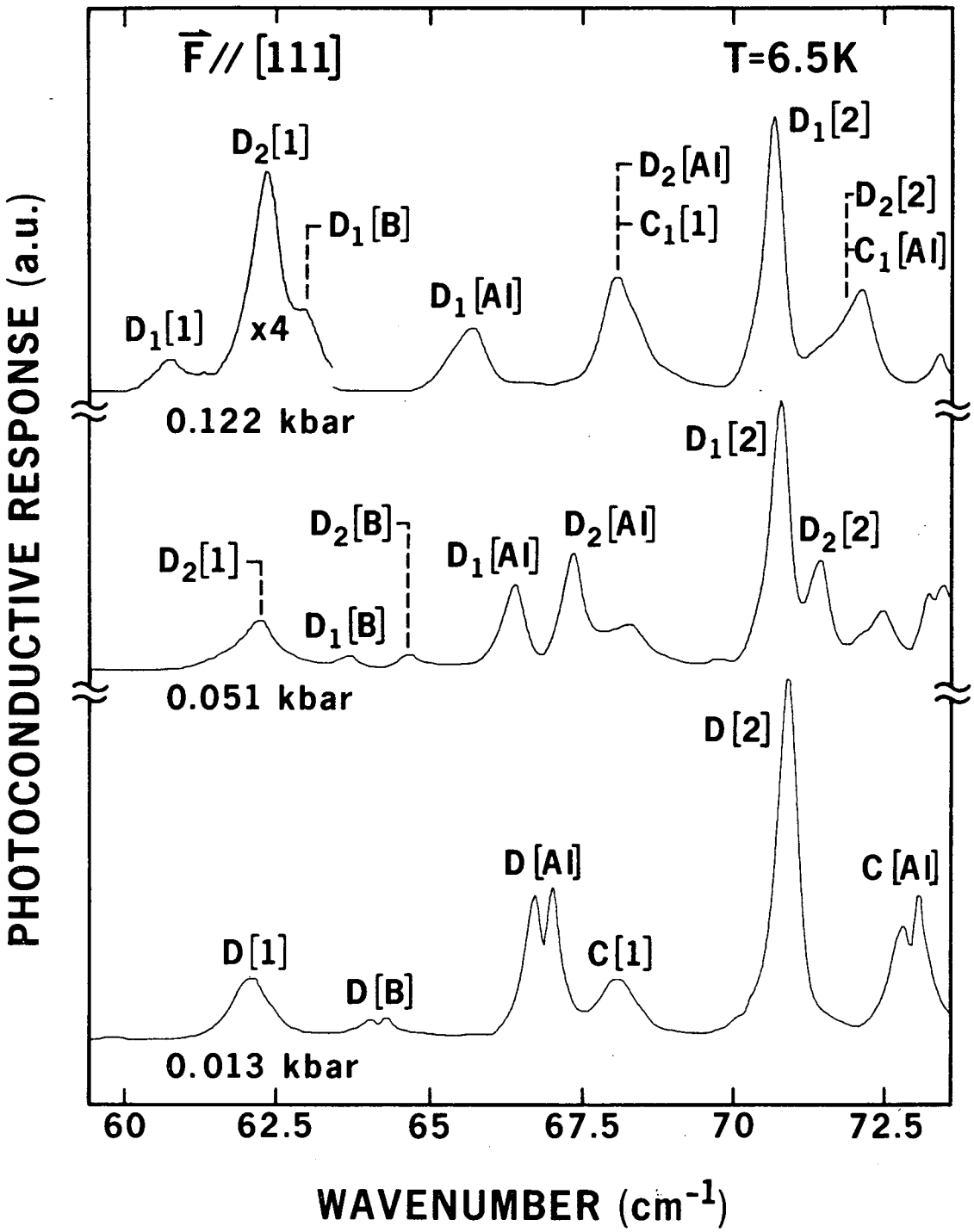

XBL 874-1719

Fig. 7.

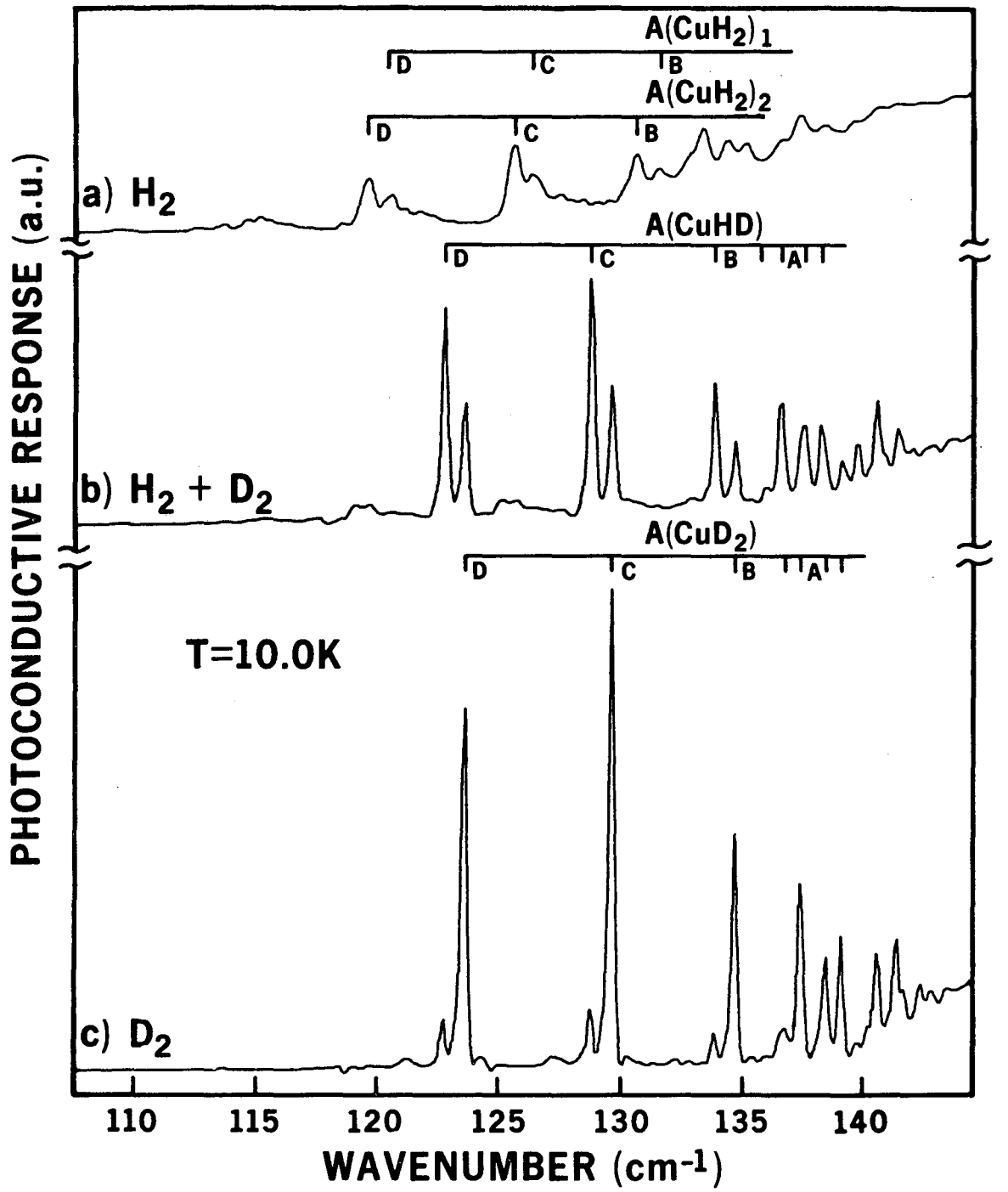

XBL 863-1157A

Fig. 8.

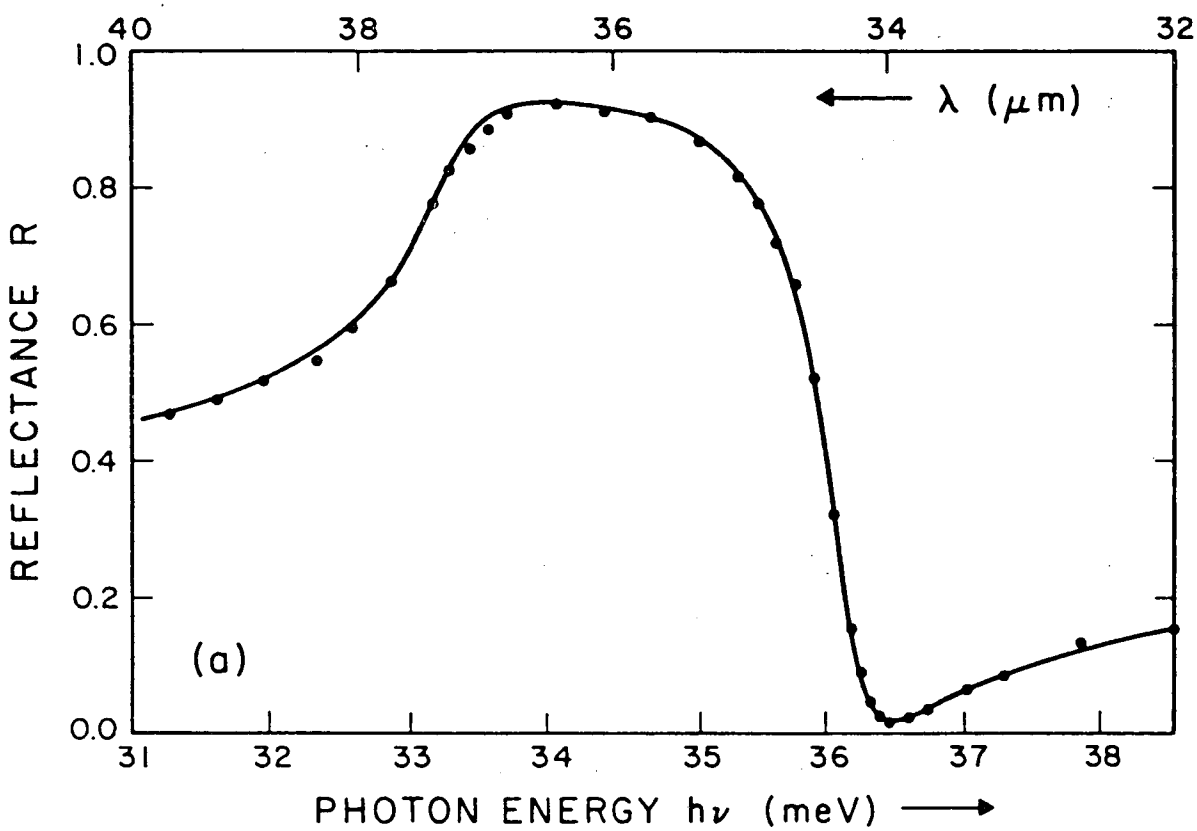

XBL 877-3345

Fig. 9.

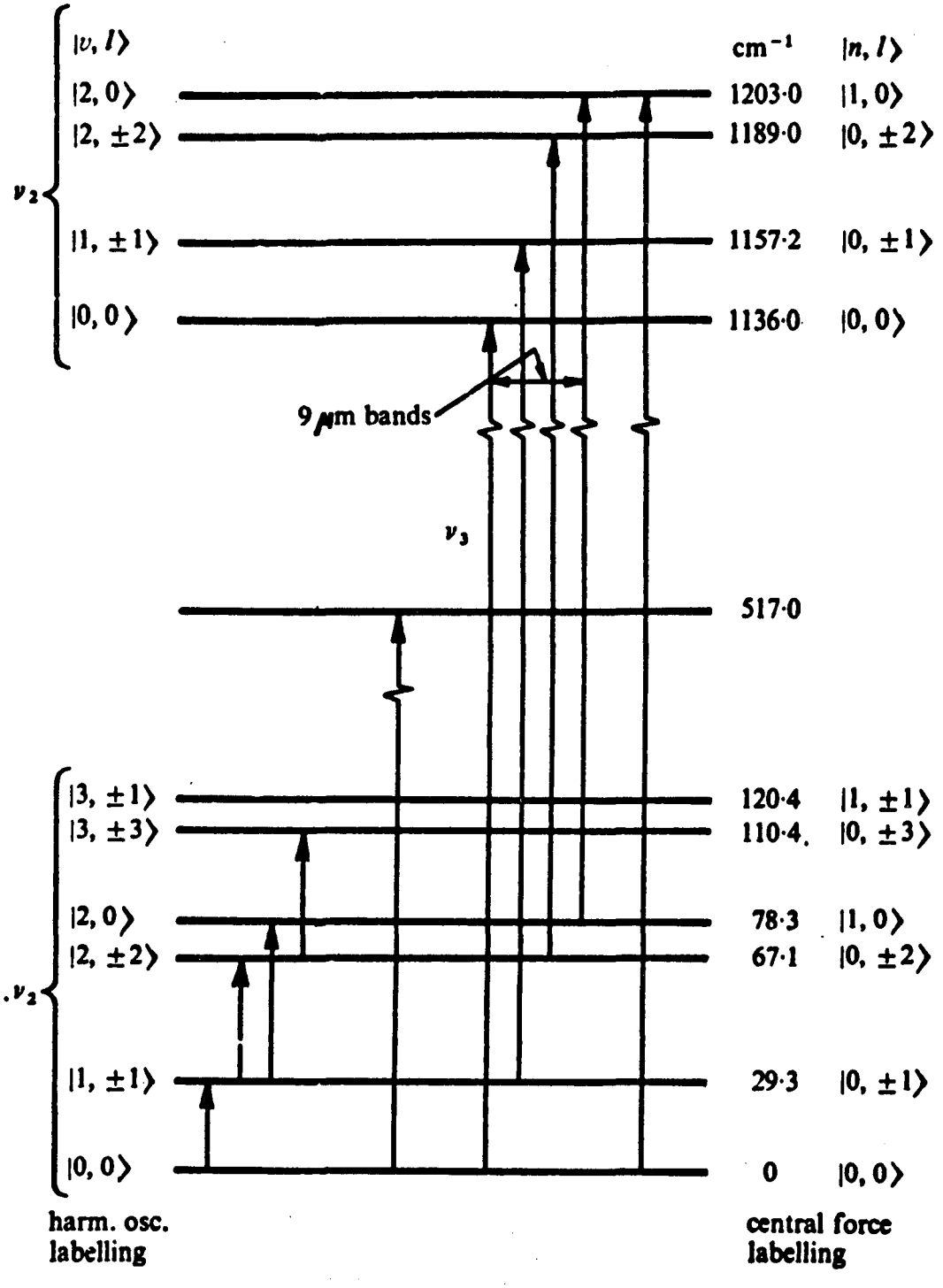
|v, l⟩
cm⁻¹
|n, l⟩
|2, 0⟩
1203·0
|1, 0⟩
|2, ±2⟩
1189·0
|0, ±2⟩
ν2
|1, ±1⟩
1157·2
|0, ±1⟩
|0, 0⟩
1136·0
|0, 0⟩
9 μm bands
ν3
517·0
|3, ±1⟩
120·4
|1, ±1⟩
|3, ±3⟩
110·4
|0, ±3⟩
|2, 0⟩
78·3
|1, 0⟩
|2, ±2⟩
67·1
|0, ±2⟩
ν2
|1, ±1⟩
29·3
|0, ±1⟩
|0, 0⟩
0
|0, 0⟩
harm. osc. labelling
central force labelling
XBL 877-3348

Fig. 10.

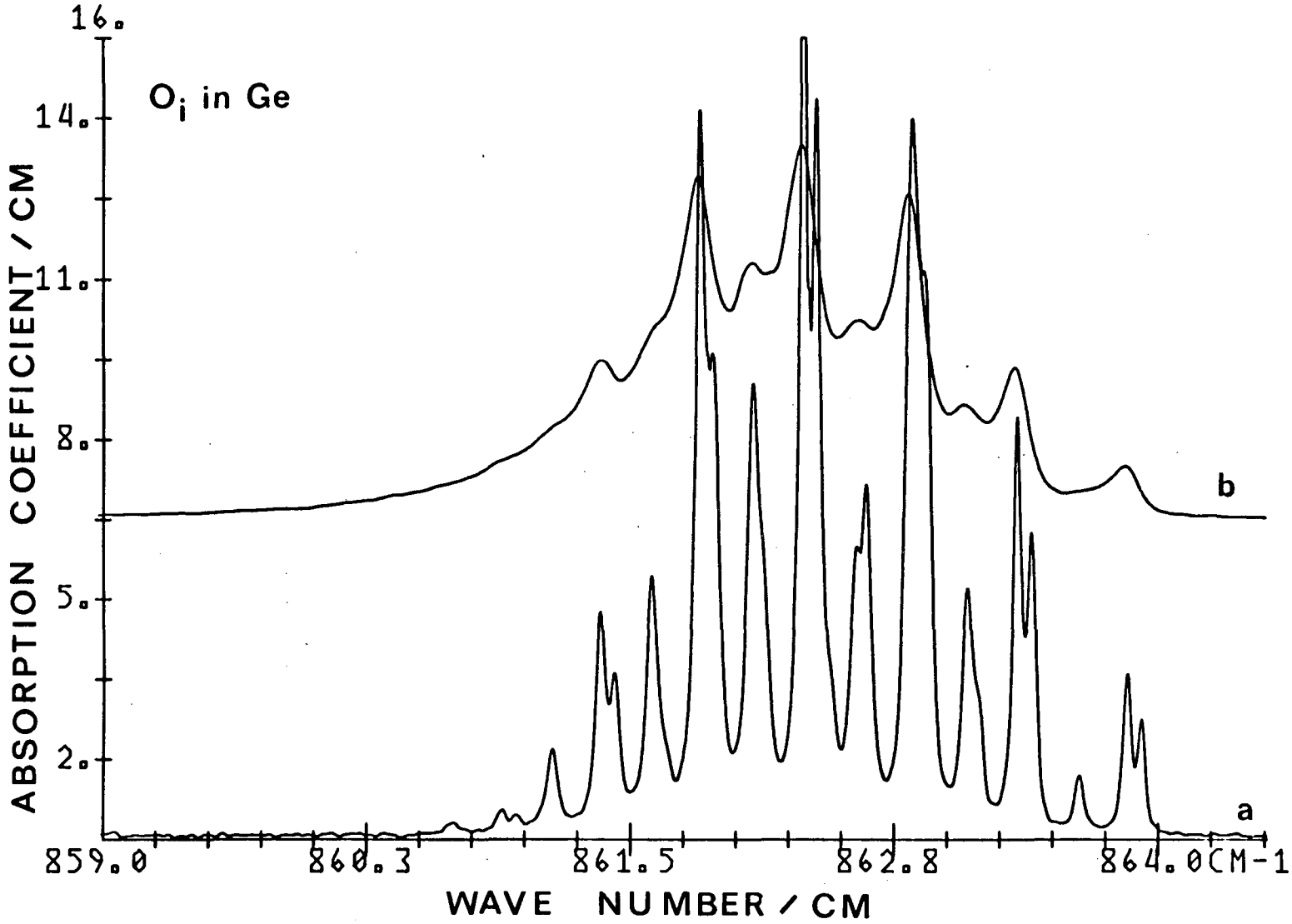
16.
14.
11.
8.
5.
2.
O_i in Ge
ABSORPTION COEFFICIENT / CM
b
a
859.0
860.3
861.5
862.8
864.0CM-1
WAVE NUMBER / CM
XBL 878-3420

Fig. 11.

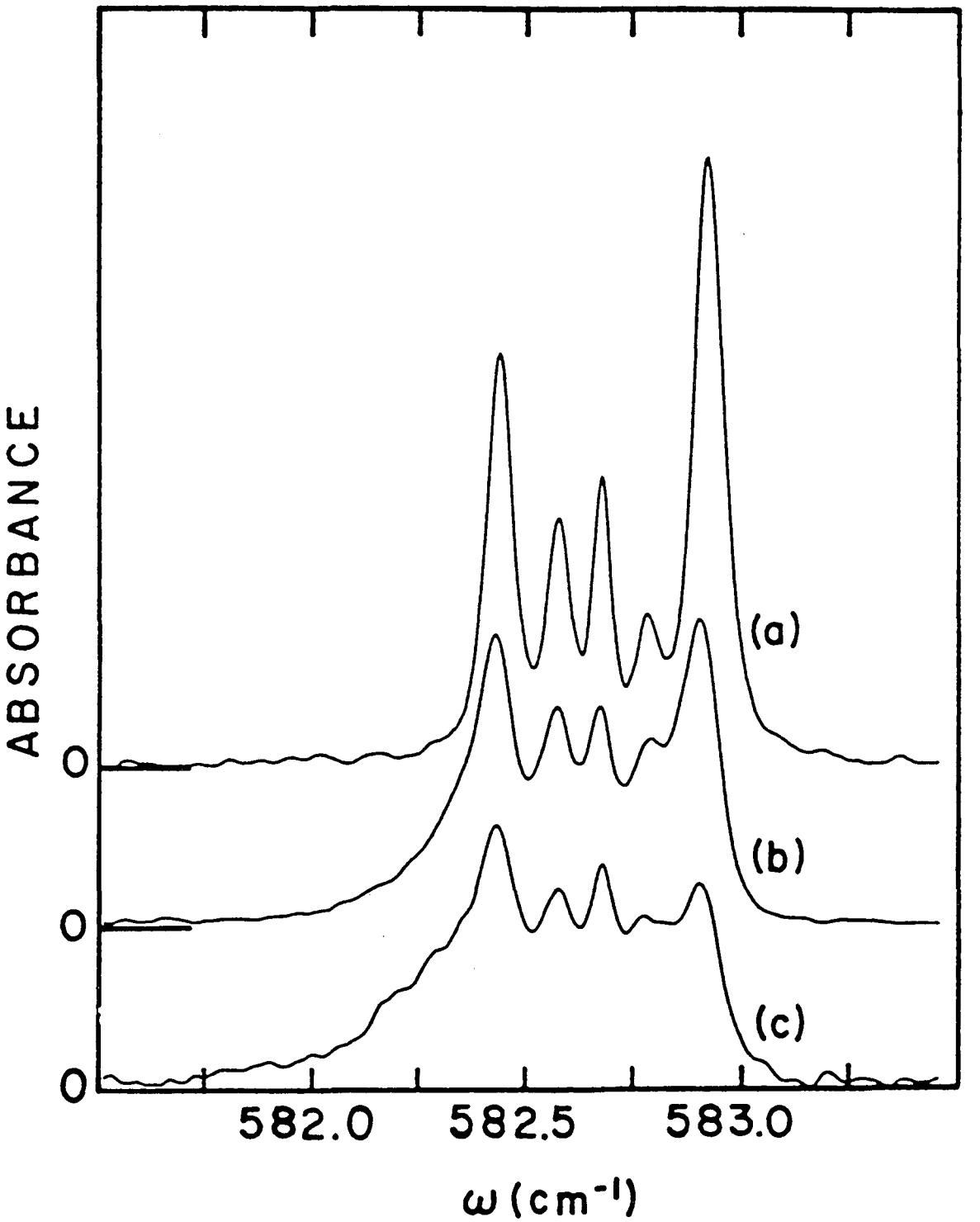

Fig. 12.

LAWRENCE BERKELEY LABORATORY
TECHNICAL INFORMATION DEPARTMENT
UNIVERSITY OF CALIFORNIA
BERKELEY, CALIFORNIA 94720